Mitochondrial Induced and Self-Monitored Intrinsic Apoptosis by Antitumor Theranostic Prodrug: In Vivo Imaging and Precise Cancer Treatment

ARTICLE *in* JOURNAL OF THE AMERICAN CHEMICAL SOCIETY · NOVEMBER 2014

Impact Factor: 12.11 · DOI: 10.1021/ja510421q · Source: PubMed

7 AUTHORS, INCLUDING:

Jiyou Han
Korea University
17 PUBLICATIONS **93** CITATIONS
SEE PROFILE

Jong-Hoon Kim
Korea University
35 PUBLICATIONS **624** CITATIONS
SEE PROFILE

JACS
JOURNAL OF THE AMERICAN CHEMICAL SOCIETY

Article

pubs.acs.org/JACS

Mitochondrial Induced and Self-Monitored Intrinsic Apoptosis by Antitumor Theranostic Prodrug: *In Vivo* Imaging and Precise Cancer Treatment

Rajesh Kumar,[†,§] Jiyou Han,[‡,§] Hee-Joung Lim,[‡] Wen Xiu Ren,[†] Ja-Yun Lim,[‡] Jong-Hoon Kim,*[,‡] and Jong Seung Kim*[,†]

[†]Department of Chemistry, Korea University, Seoul 136-701, Republic of Korea

[‡]Division of Biotechnology, Laboratory of Stem Cells and Tissue Regeneration, College of Life Sciences & Biotechnology, Korea University, Seoul 136-713, Republic of Korea

Supporting Information

ABSTRACT: Activation of apoptosis, the cell death machinery, in tumor cells by organelle-specific delivery of antitumor theranostic agent is the utmost challenge in cancer therapy. Herein, we developed a highly efficient mitochondria-targeting antitumor theranostic prodrug **7** that contained two molecules of drug 5′-deoxy-5-fluorouridine and an apoptotic marker ethidium for self-monitoring intrinsic (mitochondrial) apoptosis after its activation in tumor cells. Theranostic **7** was activated by endogenously produced mitochondrial-overexpressed H_2O_2 and released drug 5′-deoxy-5-fluorouridine and apoptotic marker ethidium to the tumor cells. The *in vitro* and *in vivo* drug release was monitored by observing the fluorescence changes of ethidium. Theranostic **7** exhibited an enhanced cytotoxicity over commercial 5-fluorouracil (an active drug of 5′-deoxy-5-fluorouridine) leading to intrinsic apoptosis monitored by in situ generated ethidium. Enhanced expression of mitochondria-mediated apoptotic genes (NOXA, PUMA, BID, BAX, and BAK), Cyt C, Caspase-3 and -9, and cell surface death receptors was observed after theranostic **7** activation in tumor cells. *In vivo* and *ex vivo* xenografts revealed that theranostic **7** significantly inhibited tumor progression and cured the tumor-bearing mice. Such organelle-specific theranostic strategies have great potential for the early diagnosis and precise treatment of cancer.

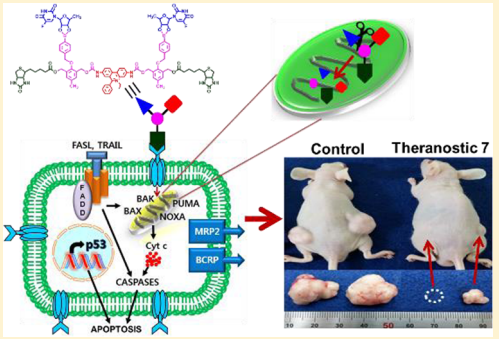

1. INTRODUCTION

The development of state-of-the-art theranostic strategies, which can help simultaneously diagnose early stage cancer, deliver therapeutic drugs to tumors, monitor drug release kinetics, and visualize cancer stages, offers techniques for effective and personalized medicine for cancer patients.[1] Combining these modalities for cancer treatment into one has the potential to prolong, localize, and minimize various toxic side effects and improve the therapeutic indexes of existing drugs.[2] Theranostic strategies are especially useful for cancer tissues that overexpress different enzymes and reactive oxygen species (ROS) and have redox imbalances that trigger the activation of diagnostics and therapeutic drugs. Because it is challenging to rationally design suitable theranostic agents, continuous efforts are needed for their development.[3]

Mitochondria, the powerhouse of cells, are the major intracellular organelles that maintain homeostasis, provide metabolic energy by oxidative phosphorylation, produce intracellular signaling by ROS, and regulate apoptosis.[4] Mitochondria simultaneously respond to different types of stimuli, including death signaling, trophic factor deprivation, DNA damage, and xenobiotics, and release mitochondria-mediated apoptotic proteins. In addition, mitochondria regulate the intrinsic apoptosis pathway that is governed by the proteins of the Bcl-2 family and followed by the activation of caspase-cascades, which lead to cell death.[5] Despite their crucial roles in normal cells, mitochondria of cancer cells function differently and have been involved in carcinogenesis and cancer progression.[6] The mitochondrial perturbations deregulate many cellular functions including enhanced metabolism, oxidative phosphorylation, and autophagy that have great impact on the cell survival or death.[7] Therefore, owing to the essential and detrimental role of mitochondria, the modulation of intrinsic apoptosis by mitochondria-targeting antitumor theranostic agents is a potential chemotherapeutic approach to eradicate cancer cells, which has not been investigated so far.

Herein, we report the design, synthesis, and development of a tumor and mitochondria-targeting antitumor theranostic prodrug **7** (Scheme 1), which delivered two molecules of prodrug in the presence of mitochondrial-overexpressed H_2O_2 and induced intrinsic (mitochondrial) apoptosis in tumor cells. Theranostic agent **7** contains four components as shown in Scheme 1. The first is a fluorophore, ethidium, that can in situ

Received: October 10, 2014

   dx.doi.org/10.1021/ja510421q | J. Am. Chem. Soc. XXXX, XXX, XXX−XXX

Scheme 1. Design and Synthesis of Theranostic Prodrug 7

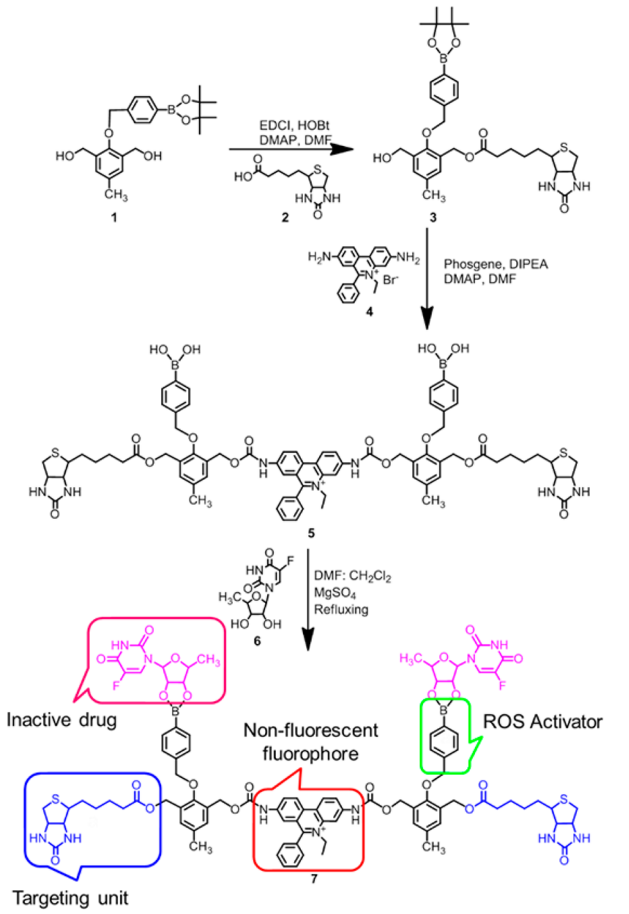

monitor intrinsic apoptosis upon drug activation. Ethidium is a fluorophore that is preferably localized in mitochondria; it is weakly fluorescent in aqueous solution and strongly fluorescent on intercalation with double-stranded RNA or DNA.[8] The second is a tumor-targeting unit, which guides theranostic **7** to tumor tissues. The third is aberrant mitochondrial-overexpressed ROS activator,[9] which activates theranostic agent **7** in cancer cells. The fourth component is an inactive drug, 5′-deoxy-5-fluorouridine (5′-DFUR), which, in the presence of thymidine phosphorylase in high concentrations in the carcinoma cells, is converted into the active drug, 5-fluorouracil (5′-FU),[10] a potent cytotoxic drug used in cancer treatment. However, its limited safety profile and high drug resistance restrict its clinical use. Therefore, the prodrug of 5′-FU, 5′-DFUR, has been utilized to increase the bioavailability and efficacy of the active drug. Theranostic **7** was selectively uptaken by the tumor cells, activated by endogenously produced mitochondrial H_2O_2, and the drug 5′-deoxy-5-fluorouridine was released to the tumor site. The *in vitro* and *in vivo* prodrug release was monitored by in situ generated fluorescent apoptotic ethidium. After drug activation in mitochondria, theranostic **7** induced intrinsic apoptosis in tumor cells followed by the activation of genomic DNA or RNA damage pathways. A remarkable suppression of tumor growth was observed after treatment with theranostic **7** in a xenograft mouse model. To our knowledge, this is the first report of mitochondria-targeting antitumor theranostic agent that upon activation permits self-monitoring apoptosis of cancer cells leading to precise cancer treatment.

2. RESULTS AND DISCUSSION

The theranostic prodrug **7** was synthesized as shown in Scheme 1. The EDCI coupling of boronic ester **1**[11] with biotin **2** in DMF produced compound **3** with a 55% yield. The subsequent reaction of **3** with ethidium bromide **4** in the presence of phosgene produced compound **5** (37%). Finally, compound **5** was conjugated to 5′-DFUR in the presence of $MgSO_4$ to produce the theranostic prodrug **7** with a 27% yield. Reference compound **10** was synthesized by the reaction of ethidium bromide **4** with 4-(hydroxymethyl)phenylboronic acid **8** in the presence of phosgene followed by 5′-DFUR conjugation in the presence of $MgSO_4$ (Scheme S1, Supporting Information). All of the compounds were characterized by ^1H and ^{13}C NMR spectroscopy, electrospray ionization-mass spectrometry (MS), and FAB-MS analyses (Figures S1−S11, Supporting Information).

For effective drug release at the tumor site, we utilized a boronic ester linkage to conjugate the prodrug with the fluorophore and targeting unit. Boronic esters react with H_2O_2, which is present at elevated levels (5 μM to 1.0 mM) in cancer cells and is an ideal target for prodrug activation.[12] Few reports have utilized a ROS-activated prodrug strategy,[13] and none used theranostic agent activation. The specificity of theranostic **7** toward H_2O_2 and prodrug activation was investigated through spectral changes under physiological conditions with ultraviolet−visible and fluorescent spectroscopy. Theranostic **7** exhibited a strong absorption band at 285 nm and a weak band at around 400 nm (Figure S12, Supporting Information). The addition of H_2O_2 to the solution of theranostic **7** and calf thymus DNA (CT-DNA) increased the absorption band at 285 nm. As expected, theranostic **7** exhibited very weak fluorescence with and without CT-DNA because caging the amino groups of ethidium dye with appropriate protecting groups hinders their DNA-binding ability.[14] However, adding H_2O_2 (500 μM) to theranostic **7** (10 μM) and CT-DNA (50 μg/mL) solution significantly increased fluorescence at 590 nm (Figure 1b and Figure S13, Supporting Information). In the presence of H_2O_2, the boronic ester groups of theranostic **7** were oxidized and hydrolyzed to corresponding phenols.[15] Theranostic **7** then started the cascade of events and released 5′-DFUR and ethidium, which intercalated with CT-DNA to give strong fluorescence (Figure 1a,b). The time-dependent fluorescence enhancement at 590 nm directly correlated with the amount of drug released from theranostic **7**, which was maximal after 24 h (Figure S13b, Supporting Information). No significant changes in theranostic **7**'s fluorescence spectra were observed in the presence of various thiols and other ROS, indicating its high selectivity for H_2O_2 (Figure S14, Supporting Information). Furthermore, theranostic **7** was stable under physiological pH (2−10) and activated only by H_2O_2 in the pH range 5−8 (Figure 1c). Reference compounds **5** (without drug) and **10** (without biotin) showed similar fluorescence behavior with CT-DNA and H_2O_2 (Figure S15, Supporting Information). The release of 5′-DFUR and ethidium from **7** after reaction with H_2O_2 was investigated with fast atom bombardment MS, and two MS peaks were observed at 245.1 $(M - H)^+$ and 314.2 $(M)^+$, corresponding to 5′-DFUR and ethidium, respectively (Figure S16, Supporting Information). These results confirmed theranostic **7** activation by H_2O_2 and the release of 5′-DFUR and ethidium. Thus, this could be an efficient drug delivery system *in vitro* as well as *in vivo*.

dx.doi.org/10.1021/ja510421q | J. Am. Chem. Soc. XXXX, XXX, XXX−XXX

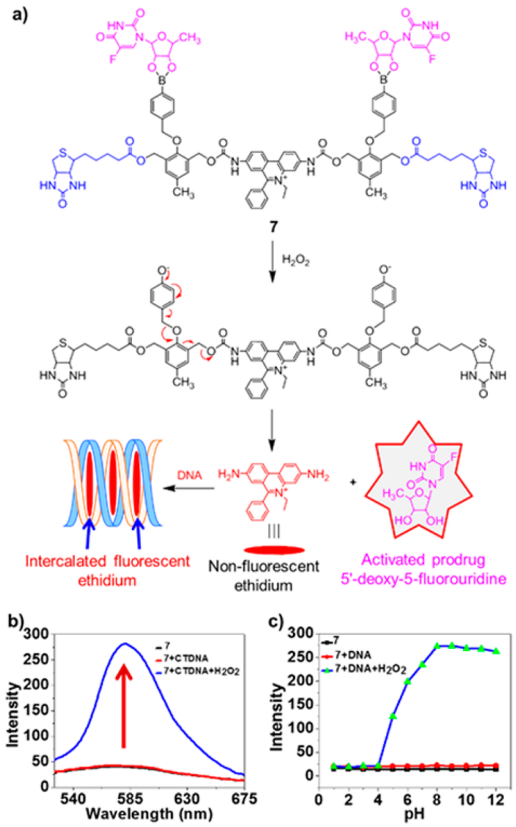

Figure 1. (a) Mechanism of drug (5′-DFUR) and fluorophore activation after reaction with H_2O_2. (b) Fluorescence spectra of theranostic 7 (10 μM) in the presence of calf thymus (CT-DNA: 50 μg/mL) and H_2O_2 (500 μM). (c) Fluorescence enhancement of theranostic 7 (10 μM) in the presence of CT-DNA (50 μg/mL) and H_2O_2 as a function of pH. λ_{ex} = 500 nm, slit width = 5,5.

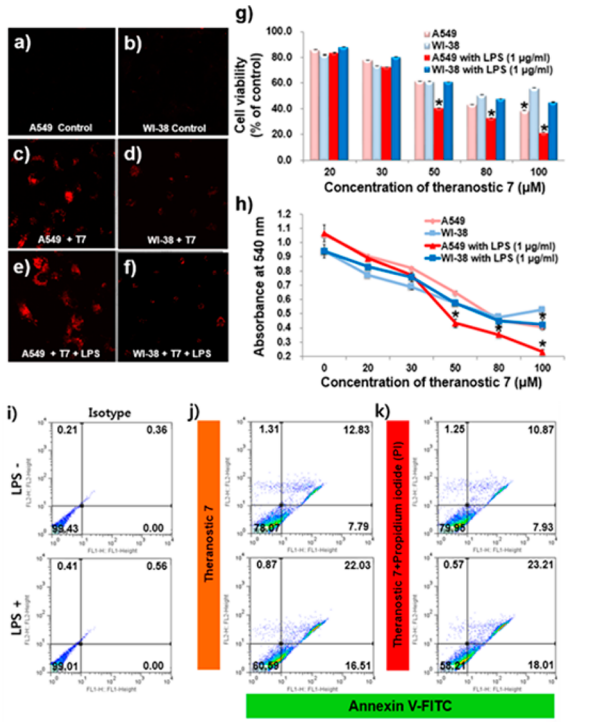

Figure 2. Cytotoxicity of theranostic 7 in A549 and WI-38 cells and the potential of theranostic 7 for fluorescence-activated cell sorting (FACS) quantitative analyses as an apoptotic dye. The cytotoxicity of theranostic 7 was examined at different concentrations (0, 20, 30, 50, 80, and 100 μM) with or without lipopolysaccharide (LPS, 1 μg/mL) as an H_2O_2 inducer. The cells were incubated for 24 h, and MTT assay was performed. (a)−(f) Fluorescent images of biotin receptor-positive A549 cells and biotin receptor-negative WI-38 cells shown at 200× magnification. (g) The percentage of cell viability in the MTT assay with various compound conditions. (h) Absorbance in the MTT assay measured at 540 nm. (i) Isotypes of theranostic 7 with or without LPS (1 μg/mL). (j) Quantitative FACS analysis of annexin V- and theranostic 7-stained early and late apoptotic cells. (k) Quantitative FACS analysis of annexin V- and PI-stained early and late apoptotic cells. (l) The results of the cell cycle distribution analysis by FACS.

For the *in vitro* investigations, we used biotin receptor-positive cells (A549 human lung cancer cells) and biotin receptor-negative cells (WI-38 human normal embryonic lung fibroblasts) and incubated them with 7 for 6 h. The presence of the cancer-guiding group (biotin) led to preferential uptake of theranostic 7 by biotin receptor-positive A549 cells, which showed significantly stronger fluorescence (Figure 2c) than the biotin receptor-negative WI-38 cells (Figure 2d). This indicated a significant tumor-targeting effect of biotin, which interacted with biotin receptor-positive carcinoma cells (A549). The increased fluorescence intensity of A549 cells further indicated the efficient activation of theranostic 7 by endogenous H_2O_2 in the tumor cells without any external inducer. To date, only a few probes detect endogenously produced H_2O_2 in tumor cells without an external inducer.[16] Furthermore, A549 cell stimulation with lipopolysaccharide (LPS) increased H_2O_2 generation in the cell, which increased the fluorescence intensity, indicating the efficiency of theranostic 7 for acute inflammation (Figure 2e,f).

The *in vitro* cytotoxicity of theranostic 7 against A549 and WI-38 cells, reference compounds **5** (without drug) and **10** (without biotin), and 5′-FU (active drug) was evaluated with or without LPS in cell viability experiments. Noticeably, theranostic 7 exhibited significantly higher cytotoxicity only for biotin receptor-positive carcinoma cells (A549) and not for biotin receptor-negative normal cells (WI-38) (Figure 2g,h). Moreover, with concentration increases from 50 to 100 μM of theranostic 7, the cytotoxicity was sharply enhanced. In addition, reference compound **5** (without drug) did not exhibit any cytotoxicity to either A549 or WI-38 cells (Figure S17a, Supporting Information). Compound **10** (without biotin) showed cytotoxicity to both carcinoma and normal cells without any cell preference, which indicated its cellular uptake through a simple diffusion method (Figure S17b, Supporting Information). However, the cytotoxicity of 5′-FU at 50 μM significantly decreased normal cell viability (approximately 52%, Figure S18, Supporting Information). Taken together, these results validated that theranostic 7 selectively went to cancer cells and exhibited approximately 20% enhanced cytotoxicity over commercial 5′-FU, leading to apoptosis.

Following cytotoxicity evaluation, theranostic 7 was successfully used for quantitative analyses of apoptotic cells with fluorescence-activated cell sorting in which ethidium, which is released from theranostic 7 after endogenous H_2O_2 activation, was utilized as a substitute for propidium iodide (PI), a widely used nuclear fluorescent dye for late apoptotic cells.[17] Our data showed 12.83% theranostic 7-stained apoptotic cells compared to 10.87% PI-stained cells, regardless of annexin V-positive cells (Figure 2j,k). These results validated the design strategy of theranostic 7 for self-monitoring of apoptosis after drug activation at the tumor site.

dx.doi.org/10.1021/ja510421q | J. Am. Chem. Soc. XXXX, XXX, XXX−XXX

Based on the tumor-specific delivery and inhibition of A549 cancer cell proliferation, the intracellular location of theranostic 7 and its apoptosis-inducing activity were evaluated (Figure 3).

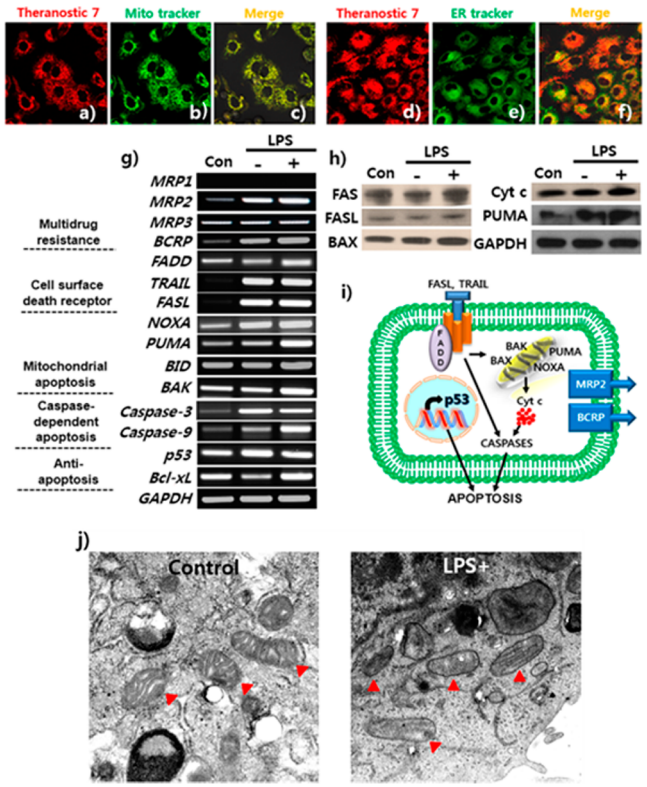

Figure 3. Intracellular localization and proapoptotic action of theranostic 7. (a–f) Theranostic 7 colocalized completely with the Mito-tracker and partially with the ER-tracker in A549 cells after a 12 h incubation with theranostic 7 (50 μM). (g) The expression of drug transporters and proapoptotic and antiapoptotic genes assessed by reverse transcription-polymerase chain reaction. (h) Alternation of death receptors and mitochondria-mediated apoptotic proteins confirmed by Western blotting. (i) Schematic mode of action of theranostic 7. The intrinsic mode of apoptotic action of theranostic 7 through mitochondria-mediated cell death and DNA integration was suggested from the increased expressions of mitochondrial apoptotic genes (BAX, BAK, NOXA, and PUMA), cytochrome C (Cyt C), and cell surface death receptors (FAS, TRAIL, and FADD). (j) Ultrastructure of mitochondria in control vs theranostic 7 with LPS-inducer treated cells. The red arrows indicate the typical mitochondrial crista structure in the control (left panel) vs the remaining mitochondrial outer membrane of the destroyed crista structure (right panel). 10000× magnification.

Theranostic 7 was visualized as red (Figure 3a,d), and the Mito-tracker and ER-tracker were visualized as green (Figure 3b,e). The organelle-specific location of theranostic 7 was confirmed from the merged images of theranostic 7 and the trackers (Figure 3c,f). The merged image (c) showed a noticeable yellow area compared to the (f) images, indicating that theranostic 7 was localized in the mitochondria, where it was activated by H_2O_2 and released 5′-DFUR.

The main mode of action of 5′-FU was to impede DNA synthesis and repair by irreversibly inhibiting thymidylate synthase, thus slowing tumor growth.[18] Additionally, 5′-FU metabolites incorporated into DNA and RNA structures further induce apoptosis. Interestingly, the mode of action of theranostic 7, which contains prodrug 5′-DFUR of 5′-FU, was altered with significantly improved anticancer efficacy. Theranostic 7 was colocalized and activated in the mitochondria rather than in cytoplasm or nuclei (Figure 3a–f), thereby producing different modes of action.

To validate the different mode of action, we investigated the anticancer effects of theranostic 7 on the expression of mitochondria-mediated apoptotic genes [NOXA, p53-upregulated modulator of apoptosis (PUMA), BID, BAX, and BAK] by polymerase chain reaction and Western blotting. Apoptotic genes were upregulated by theranostic 7 and further enhanced by the LPS inducer (Figure 3g,h). These genes are members of the BH3-only proapoptotic protein of Bcl-2 superfamily, which possesses Bcl-2 homology (BH) domains (BH1 to BH4). NOXA is a BH3 only pro-apoptotic protein that causes mitochondrial fragmentation,[19] whereas BID, BIM, and PUMA are important for stimulation of BAX/BAK-induced mitochondrial apoptosis.[20] These upregulated genes play crucial roles in mitochondrial dysfunction and facilitate apoptosis.[21]

Intriguingly, an increased expression of p53 was observed with/without LPS inducer (Figure 3g). The most important contribution of p53 to apoptosis is reliant on transcriptional activation of a key subset of proapoptotic Bcl-2 family genes, including BAX, NOXA, PUMA, and BID.[22] In compliance, our data showed p53-reliant apoptosis activated a mitochondrial pathway, antagonizing Bcl-xL and eventually disrupting mitochondrial structure (Figure 3j, red arrowheads). Thus, theranostic 7 induces the mitochondria-mediated pathway of apoptosis prior to inhibiting DNA synthesis and repair.

In addition to mitochondria-mediated apoptotic genes, the upregulation of Cyt C, an intermembrane space protein, from mitochondria was observed (Figure 3h) and subsequently activated caspase-dependent apoptosis.[23] Concordantly, Caspase-3 and -9 expressions were significantly upregulated by theranostic 7 (Figure 3g). These results indicated that theranostic 7 exhibited intrinsic apoptotic induction in cancer cells by the mitochondria-mediated pathway and then by integrating into the nuclear RNA and DNA of cancer cells.

Furthermore, theranostic 7 increased the expression of cell surface death receptors such as FADD, FAS, FASL, and TRAIL receptors, which further induced apoptosis signaling pathways (Figure 3g). These findings were very significant for understanding the mode of action of 5′-FU on cell surface death receptors, the knowledge of which is relatively obscure. Additionally, inflection of TRAIL receptor signaling in tumor cells caused by anticancer drug determine the chemosensitivity of drug, reduction in tumor regression, and clearance.[24] Even though further analyses are needed to validate the potential effects of increased TRAIL and FasL on apoptosis, we speculate that theranostic 7 significantly increases the chemosensitivity of 5′-FU.

Despite the many advantages of 5′-FU treatment, its overall response rate to cancer is relatively low (10%–30%), even when administrated with other anticancer drugs such as irinotecan and oxaliplatin (50%) due to increased drug efflux that leads to chemoresistance.[25−27] The expression of multidrug resistance proteins (MRP) and breast cancer resistance protein (BCRP), the drug efflux transporters, have been investigated as a result. MRP2 and BCRP, but not MRP1 and MRP3, exhibited increased expression with theranostic 7 (Figure 3g). 5′-FU induces MRP5 expression in colorectal and breast cancers,[28] but it has never been reported to upregulate the BCRP and MRP2 in lung cancer cells, which is significant to understanding the drug resistance mechanism. Despite the

dx.doi.org/10.1021/ja510421q | J. Am. Chem. Soc. XXXX, XXX, XXX–XXX

BCRP and MRP2 upregulation, theranostic 7 showed stronger anticancer effects than 5′-FU alone due to its cancer-targeting effect, intrinsic apoptotic induction, and large molecular weight that prevented its cell leakage.

Finally, *in vivo* studies were performed at 4 weeks to evaluate the tumor target specificity, organ distribution, and antitumor activity of theranostic 7 with A549-inoculated xenograft mice. The xenograft mice were administrated theranostic 7 by tail-vein injections, and images were taken noninvasively after 4.5 h. Enhanced fluorescence signals were observed in tumor tissue activated by endogenous H_2O_2, validating the strong tumor-targeting effect. Fluorescence signals were increased when LPS (10 μL, 1.0 μg/mL) was injected directly into the tumor tissue of the right side 1 h after the theranostic 7 tail-vein injection (Figure 4a). To confirm the targeted effect of theranostic 7 and

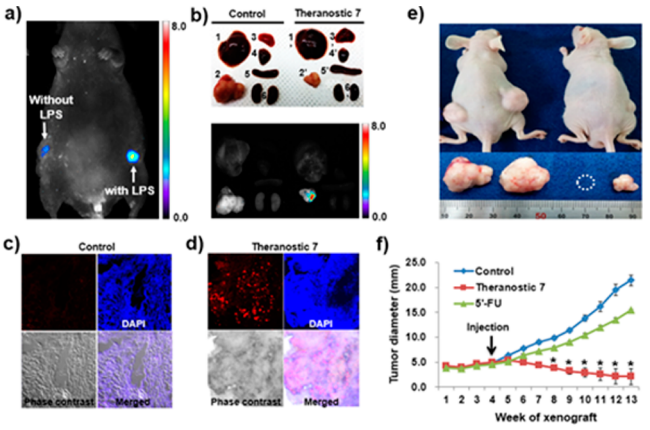

Figure 4. Chemotherapeutic effects of theranostic 7 in *in vivo*/*ex vivo* xenograft mouse models. After 4 weeks of inoculation with A549 human lung carcinoma cells, the xenograft mice were tail-vein-injected with PBS or theranostic 7 (2 mM) once a week for 9 weeks. (a) Representative fluorescent *in vivo* images of theranostic 7 in xenograft mouse after 4 weeks of inoculation. The image was taken 4.5 h after tail-vein injections. Ten microliters (1 μg/mL) of LPS-inducer for H_2O_2 production was injected into the right side of the tumor 1 h after the theranostic 7 injection. (b) *Ex vivo*-dissected organs and optical fluorescent images of the control- and theranostic 7-injected xenograft mice 13 weeks after inoculation. Liver (1 and 1′), tumor tissue (2 and 2′), lung (3 and 3′), heart (4 and 4′), spleen (5 and 5′), and kidney (6 and 6′). (c), (d) Fluorescent intracellular image of tumor cryosections from control- and theranostic 7-injected xenograft mice, respectively. Magnification: 200×. (e) Effects of theranostic 7 on *in vivo* tumor progression in control- and theranostic 7-injected xenograft mice and dissected tumor tissues 9 weeks after initiation. (f) Growth of tumors in xenograft mice. A549 cells were subcutaneously injected into BALB/cN nude mice (n = 8). Tumors were measured weekly for 13 weeks, and tumor growth curves were constructed to compare the tumor sizes among the PBS-, 5′-FU-, and theranostic 7-injected groups.

its activation at the organ level, the tumors and normal tissues of control and theranostic 7-injected mice were dissected. *Ex vivo* imaging clearly showed the specific uptake of theranostic 7 and its activation at the tumor site over other organs, including the liver, lung, heart, spleen, and kidney (Figure 4b). Furthermore, stronger and more evenly distributed fluorescent signals were observed in cryosectioned tumor tissues of theranostic 7-injected mice than in control tumor tissues (Figure 4c,d). The tumor fluorescence intensity was approximately 7-fold that of normal tissues. Our data clearly indicated the more effective tumor targeting of theranostic 7 over that of normal tissues.

To demonstrate the antitumor effects, theranostic 7 (2 mM per mouse in 0.1 mL of PBS) was administered by tail-vein injections into A549-inoculated xenograft mice every week for 13 doses, after which tumor growth was observed. Tumor growth was remarkably suppressed by theranostic 7 treatment compared to the case with the controls (Figure 4e). The antitumor efficacy of theranostic 7 was so strong that a tumor on the left thigh of a mouse was completely suppressed and a tumor on the right thigh was significantly reduced. Furthermore, the tumor growth was significantly inhibited 8 weeks after the theranostic 7 injection (Figure 4f). Taken together, we validated that theranostic 7 preferentially targeted the target site where it accumulated and was visualized and was activated by endogenous H_2O_2 to deliver the prodrug to the cancer cells. The prodrug was then specifically converted into active drug in the cancer cells, resulting in apoptosis and, eventually, the inhibition of tumor growth in *in vivo* tumor models.

3. CONCLUSIONS

In summary, we successfully developed ethidium-prodrug 7 as an effective theranostic agent capable of tumor and mitochondria-targeting, diagnosis, and prodrug delivery to the tumor site. *In vitro* cellular results showed an enhanced anticancer efficacy of theranostic 7, which contained the 5′-FU prodrug and induced the intrinsic apoptotic pathway that was followed by nuclear DNA or RNA damage in the tumor cells. The *in vivo* and *ex vivo* xenograft mouse model showed tumor inhibition, and the animal was cured. Future management may lie in all-in-one organelle-specific theranostic strategies for cancer therapy through careful selection of modified DDS conjugated with anticancer drugs based on the likelihood of response and the development of resistance.

4. EXPERIMENTAL SECTION

Materials and Spectroscopic Methods. For all reactions, chemicals were obtained from Aldrich, Acros Organics, Carbosynth, TCI, and Alfa-Aesar. These chemicals were used without any further purification. For reaction progress monitoring and column chromatography, Merck F254 TLC plates and Silica gel 60 were used, respectively. The ^{1}H and ^{13}C NMR spectra were recorded on Varian 300 and 400 MHz spectrometers using $CDCl_3$, DMSO-d_6, and CD_3OD, with TMS used as an internal reference. Thermo Scientific LTQ Orbitrap Mass Spectrometer was used to obtain ESI-MS spectra.

Absorption and Fluorescence Measurements. The working solutions of compounds **5**, **7**, and **10**, using triple-distilled water, were prepared from their stock solutions (1.0 mM) in DMSO. All spectra were recorded under physiological conditions (DMSO: PBS; 0.5:9.5, v/v, pH 7.4, 37 °C). A Scinco S-3100 spectrophotometer was used to record the absorption spectra using 20 μM compounds. A Shimadzu RFPC-5301 spectrofluorometer was used for recording the fluorescence spectra using 10 μM compounds with excitation and emission slit widths of 5 and 5 nm, respectively, and excitation wavelength of 500 nm. The calf thymus DNA (CT-DNA) was dissolved in triple-distilled water and stored at −20 °C. For the solution tests of compounds **5**, **7**, and **10**, 500 μM samples of different reactive oxygen species were used.

dx.doi.org/10.1021/ja510421q | J. Am. Chem. Soc. XXXX, XXX, XXX−XXX

Hydrogen peroxide (H_2O_2), hypochlorite ion (OCl^-), and *tert*-butyl hydroperoxide (TBHP) were used as commercially available aqueous solutions of 30%, 5%, and 70%. Solid KO_2 was used as a source of superoxide (O^{2-}). For obtaining the *tert*-butoxy radical ($^{\bullet}O^tBu$) and hydroxyl radical ($^{\bullet}OH$) 1 mM Fe^{2+} was reacted with 500 μM TBHP or 500 μM H_2O_2, respectively.

Cell Culture, Reagents, and Imaging. The human lung carcinoma cells (A549) and normal lung fibroblast cells (WI-38) were obtained from Korean Cell Line Bank (Seoul, Republic of Korea) and the American Type Culture Collection. Medium RPMI 1640 (GIBCO BRL, Grand Island, NY, USA) was used for the cells culture, supplemented with 10% fetal bovine serum (FBS, GIBCO), 1% penicillin (GIBCO), and streptomycin (GIBCO) at 37 °C in a 5% CO_2 and 95% air environment. When the cell density reached 70−80% of confluence, a subculture was done and the medium was changed approximately every 3 days.

Cells were seeded on a 35 mm confocal dish (glass bottom dish, SPL, Kyong-Gi, Republic of Korea) at a cell density of 2.0 × 106 per 35 mm and stabilized for 48 h. Prior to examining fluorescent images, we treated various concentrations of theranostic 7 in 2 mL of culture media without FBS with biotin receptor-positive A549 cells and biotin receptor-negative WI-38 cells for 24 h at 37 °C in a 5% CO_2 and 95% air environment. Then cells were washed with 1 mL of PBS twice. Theranostic 7 (50 μM, in 10 μL of DMSO per 2 mL of media in a 35 mm dish) was added to the culture media for 6 or 24 h, and cells were again washed twice with 1 mL of PBS. A confocal laser scanning microscope (Carl-Zeiss LSM 5 Exciter, Oberko, Germany), equipped with a 480 nm Ar laser and 580 nm long pass filter, was used to get the fluorescence images. Unless otherwise stated, all fluorescence images of cells and tissues were recorded under the same conditions. The fluorescence for theranostic 7 was excited at 500 nm, and emission was collected by a 650 nm band-pass filter. For the fluorescence of Mito-tracker and ER-tracker, the red fluorescence was excited at 405 nm and the emission was collected by a 545−560 nm filter. The collected data was analyzed using 3D deconvolution process of MetaMorph Offline software (Version 7.6.1, Molecular Devices, Sunnyvale, CA, USA).

Cytotoxicity Evaluation. The sensitivity and cytotoxicity of the theranostic 7 were examined and compared between carcinoma cells and normal cells. Both A549 (biotin receptor-positive cell line) and WI-38 (biotin receptor-negative cell line) were washed with 1 mL of PBS twice and the FBS-free RPMI and DMEM culture media changed prior to assay. The cell viability of theranostic 7 was tested by the MTT (3-(4,5-dimethylthiazol-2-yl)-2,5 diphenyltetrazolium bromide, Life Technologies, Carlsbad, CA, USA) assay per the manufacture's instruction. Briefly, A549 and WI-38 cells (1.5 × 104 cells in 100 mL of media) were seeded onto a 96-well plate. On the following day, the culture medium was changed with different concentrations (0, 20, 30, 50, 80, and 100 μM) of conjugate 7 in 100 mL of fresh medium, and the cultures incubated at 37 °C for 24 h. After 24 h, 1 mL of 12 mM MTT solution was added to each well, including negative controls in the absence of conjugate 7 and a well with 1 mL of medium alone. After a 1 h incubation, the medium was removed from the wells, 500 μL of DMSO was added to each well, and they were mixed thoroughly for 15 min. The absorbance was measured at 540 nm using a microplate spectrophotometer (PowerWave XS, Bio-Tek, Winooski, VT, USA).

Reverse Transcription PCR (RT-PCR). For RT-PCR analysis, TRIzol Reagent (Invitrogen) and the reverse transcription system (Promega, Madison, WI, USA) were used to isolate the total RNA from cells by following the protocols of the manufacturer. The amplification of genes was done using EXTaq polymerase (Takara). The primers and PCR conditions applied are given in Table S1, Supporting Information.

Western Blotting. After the ice-cooled PBS washing (twice) of the protein (~80% confluent), cells were lysed in RIPA lysis buffer (100 μL, Upstate, Lake Placid, NY, USA) containing a cocktail tablet of protease inhibitors (Roche Diagnostics GmbH, Mannheim, Germany). Bradford assay using a Bio-Rad protein assay kit (Bio-Rad) was used to measure the concentration of the protein. SDS-PAGE gels (12%, mini precast TDX-gel, Bio-Rad) were used to obtain the same amount of protein (60 μg/lane) that was then moved to nitrocellulose membranes (Schleicher & Schull, Dassel, Germany). Tween 20 (TBST) and 5% nonfat dry milk in Tris-buffered saline were used to block the membrane for 1 h, and the membrane was incubated overnight with primary antibody at 4 °C (Table S2, Supporting Information). The membranes were washed three times for 10 min in TBST containing 0.1% Tween 20 and incubation was performed with peroxidase-conjugated secondary antibody at room temperature for 1.5 h (1:2000, Jackson ImmunoResearch Laboratories). Membranes were again rinsed three times for 10 min with TBST and detected using the enhanced chemiluminescence detection system (Amersham Bioscience).

Transmission Electron Microscopy (TEM). A549 cells were fixed in 2.5% glutaraldehyde−2% PFA in 0.1 M phosphate buffer (pH 7.4) at 4 °C for 2 h. The cells were rinsed with 0.1 M phosphate buffer under dark conditions, and 1% OsO_4 in 0.1 M phosphate buffer was used to postfix the cells for 1 h. Postfixed cells were then dehydrated, infiltrated with propylene, and embedded in Epon812 mixture. The blocks were cut into ultrathin sections (60 nm) using Ultracut UCT (Leica). After being stained with uranyl acetate and lead citrate, the sections were examined with the H-7600 transmission electron microscope (Hitachi).

Mouse Xenograft Model. To examine the chemotherapeutic effect and the image of theranostic 7 in the tumor tissue, 6- to 8-week-old BALB/c nude mice (control xenograft, n = 8; treatment injected xenograft, n = 8) were obtained from RaonBio (Kayonggido, Yonginsi, South Korea). All animals were acclimatized to the animal facility for at least 48 h prior to experimentation and preserved as per the "Guide for the Care and Use of Laboratory Animals" published by the NIH. They were housed in a barrier under HEPA filtration and provided with sterilized food and water *ad libitum*. They were maintained under 12 h light/dark cycles at room temperature 21 ± 2 °C with 30−40% humidity. Approximately 5.0 × 106 cells of A549 were mixed with 354234-matrigel (BD, San Jose, CA, USA) and subcutaneously injected in the right and left flanks of the mice.

***In Vivo* and *ex Vivo* Fluorescent Imaging.** *In vivo* and *ex vivo* investigations were examined to evaluate the tumor target specificity and organ distribution of theranostic 7 using A549-inoculated xenograft mice. *In vivo* spectral fluorescence images were acquired 4.5 h after theranostic 7 at 4 weeks of inoculation by using Maestro2. At one tumor site, the mice were administrated an intraperitoneal injection of 10 μL (1 μg/mL) of LPS, and after 4.5 h, 2 mM in 0.1 mL of PBS per mouse of theranostic 7 was injected via tail-vein injection. To validate

dx.doi.org/10.1021/ja510421q | J. Am. Chem. Soc. XXXX, XXX, XXX−XXX

theranostic effect, 2 mM theranostic 7 in 0.1 mL of PBS was injected into the tail-vein of xenograft mice once a week after 4 weeks of inoculation. After 9 weeks of theranostic 7 injections, the tumor tissues and other organs (lung, heart, liver, kidney, and spleen) of the control and injected mice were dissected for *ex vivo* images using Maestro2. The filter set used for both *in vivo* and *ex vivo* images was blue: excitation and emission; 500−650 nm. The fluorescence images and autofluorescence were then unmixed with commercial software (Maestro software ver. 2.4, CRi, Woburn, MA, USA) using the multiexcitation spectral analysis function.

After *ex vivo* images were taken, the grafted tumor tissues and other organs (lung, heart, liver, kidney, and spleen) were embedded in Tissue-Tek 100% optimal cutting temperature compound (O.C.T., Sakura Finetek) for cryosection. Prior to further analysis, the fresh tissue was rapidly snap frozen by placing into liquid nitrogen and storing in a −80 °C freezer. Freshly cryopreserved tissues were cut (6 μM thick) using a −25 °C ultramicrotome (Leica CM 3050 S, Wetzlar, Germany). Each section was picked up on an adhesion microscope glass slide (Paul Mariendeld GmbH & Co.KG, Lauda-Königshofen, Germany) and then carefully washed of O.C.T compound twice with PBS. The sections were incubated with 2 mM theranostic 7 for 2 h with DAPI counter staining and covered with fluorescent slide cover glass. Fluorescent images were collected with a confocal laser scanning microscope (Carl-Zeiss LSM 5 Exciter, Oberko, Germany).

Statistical Analysis. Three independent experiments performed in triplicate were used to obtain the numerical values as the mean or standard error of the mean (SEM). One-way analysis of variance (ANOVA) of the SAS program (version 8.2, Cary) was performed to evaluate statistical significance. Paired Student's *t*-tests were performed to compare the means when ANOVAs indicated a significant difference. The *P*-values were determined to be significant if less than 0.05.

■ ASSOCIATED CONTENT

Supporting Information

Synthetic and experimental details and ^{1}H and ^{13}C NMR, and ESI-MS spectra of new compounds. Additional data of UV−vis absorption, fluorescence, MS spectra, and biological evaluations. This material is available free of charge via the Internet at http://pubs.acs.org.

■ AUTHOR INFORMATION

Corresponding Authors

jhkim@korea.ac.kr

jongskim@korea.ac.kr

Author Contributions

[§]These authors contributed equally.

Funding

The authors declare no competing financial interest.

Notes

The authors declare no competing financial interest.

■ ACKNOWLEDGMENTS

This work was supported by The Ministry of Science, ICT & Future Planning (MSIP) of National Research Foundation of Korea (No. 2009-0081566 for J.S.K. and No. 2012M3A9C7050139 for J.H.K.), Korea University Grant (for J.H.) and Basic Science Research Program through the National Research Foundation of Korea (NRF) funded by the Ministry of Education (No. 2013062997).

■ REFERENCES

(1) Kelkar, S. S.; Reineke, T. M. *Bioconjugate Chem.* **2011**, *22*, 1879−1903.

(2) Chen, X.; Gambhir, S. S.; Cheon, J. *Acc. Chem. Res.* **2011**, *44*, 841−841.

(3) Svenson, S. *Mol. Pharmaceutics* **2013**, *10*, 848−856.

(4) Kroemer, G.; Galluzzi, L.; Brenner, C. *Physiol. Rev.* **2007**, *87*, 99−163.

(5) Susin, S. A.; Lorenzo, H. K.; Zamzami, N.; Marzo, I.; Snow, B. E.; Brothers, G. M.; Mangion, J.; Jacotot, E.; Costantini, P.; Loeffler, M.; Larochette, N.; Goodlett, D. R.; Aebersold, R.; Siderovski, D. P.; Penninger, J. M.; Kroemer, G. *Nature* **1999**, *397*, 441−446.

(6) (a) Gogvadze, V.; Orrenius, S.; Zhivotovsky, B. *Trends Cell Biol.* **2008**, *18*, 165−173. (b) Modica-Napolitano, J. S.; Singh, K. K. *Mitochondrion* **2004**, *4*, 755−762.

(7) Kroemer, G.; Pouyssegur, J. *Cancer Cell* **2008**, *13*, 472−482.

(8) Villa, A. M.; Doglia, S. M. *Eur. J. Cancer* **2009**, *45*, 2588−2597.

(9) Lee, S.; Tak, E.; Lee, J.; Rashid, M. A.; Murphy, M. P.; Ha, J.; Kim, S. S. *Cell Res.* **2011**, *21*, 817−834.

(10) Mori, K.; Hasegawa, M.; Nishida, M.; Toma, H.; Fukuda, M.; Kubota, T.; Nagasue, N.; Yamana, H.; Hirakawa-YS Chung, K.; Ikeda, T.; Takasaki, K.; Oka, M.; Kameyama, M.; Toi, M.; Fujii, H.; Kitamura, M.; Murai, M.; Sasaki, H.; Ozono, S.; Makuuchi, H.; Shimada, Y.; Onishi, Y.; Aoyagi, S.; Mizutani, K.; Ogawa, M.; Nakao, A.; Kinoshita, H.; Tono, T.; Imamoto, H.; Nakashima, Y.; Manabe, T. *Int. J. Oncol.* **2000**, *17*, 33−41.

(11) Lux, C. G.; Joshi-Barr, S.; Nguyen, T.; Mahmoud, E.; Schopf, E.; Fomina, N.; Almutairi, A. *J. Am. Chem. Soc.* **2012**, *134*, 15758−15764.

(12) Yang, W. Q.; Gao, X.; Wang, B. H. In *Boronic Acids;*, Hall, D. G., Ed.; Wiley-VCH Verlag GmbH & Co. KGaA: Weinheim, 2005; pp 481−512.

(13) Kuang, Y.; Balakrishnan, K.; Gandhi, V.; Peng, X. *J. Am. Chem. Soc.* **2011**, *133*, 19278−19281.

(14) Sanchez, M. I.; Martinez-Costas, J.; Gonzalez, F.; Bermudez, M. A.; Vazquez, M. E.; Mascarenas, J. L. *ACS Chem. Biol.* **2012**, *7*, 1276−1280.

(15) Kuivila, H. G.; Armour, A. G. *J. Am. Chem. Soc.* **1957**, *79*, 5659−5662.

(16) Lee, D.; Khaja, S.; Velasquez-Castano, J. C.; Dasari, M.; Sun, C.; Petros, J.; Taylor, W. R.; Murthy, N. *Nat. Mater.* **2007**, *6*, 765−769.

(17) Rieger, A. M.; Nelson, K. L.; Konowalchuk, J. D.; Barreda, D. R. *J. Visualized Exp.* **2011**, *50*, e2597.

(18) Longley, D. B.; Harkin, D. P.; Johnston, P. G. *Nat. Rev. Cancer* **2003**, *3*, 330−338.

(19) Woo, H.-N.; Seo, Y.-W.; Moon, A. R.; Jeong, S.-Y.; Jeong, S.-Y.; Choi, E. K.; Kim, T.-H. *FEBS Lett.* **2009**, *583*, 2349−2354.

(20) Ren, D.; Tu, H.-C.; Kim, H.; Wang, G. X.; Bean, G. R.; Takeuchi, O.; Jeffers, J. R.; Zambetti, G. P.; Hsieh, J. J.-D.; Cheng, E. H.-Y. *Science* **2010**, *330*, 1390−1393.

(21) Xiong, H.-Y.; Guo, X.-L.; Bu, X.-X.; Zhang, S.-S.; Ma, N.-N.; Song, J.-R.; Hu, F.; Tao, S.-F.; Sun, K.; Li, R.; Wu, M.-C.; Wei, L.-X. *Cancer Lett.* **2010**, *288*, 68−74.

(22) Yu, J.; Zhang, L. *Cancer Cell* **2003**, *4*, 321−328.

(23) Gallego, M.-A.; Joseph, B.; Hemstrom, T. H.; Tamiji, S.; Mortier, L.; Kroemer, G.; Formstecher, P.; Zhivotovsky, B.; Marchetti, P. *Oncogene* **2004**, *23*, 6282−6291.

(24) Menke, C.; Goncharov, T.; Qamar, L.; Korch, C.; Ford, H. L.; Behbakht, K.; Thorburn, A. *PLoS One* **2011**, *6*, e14527.

(25) Douillard, J. Y.; Cunningham, D.; Roth, A. D.; Navarro, M.; James, R. D.; Karasek, P.; Jandik, P.; Iveson, T.; Carmichael, J.; Alakl, M.; Ruia, G. G.; Awad, L.; Roug, P. *Lancet* **2000**, *355*, 1041−1047.

(26) Zhang, N.; Yin, Y.; Xu, S.-J.; Chen, W.-S. *Molecules* **2008**, *13*, 1551−1569.

(27) Horiguchi, S.; Shiraha, H.; Nagahara, T.; Kataoka, J.; Iwamuro, M.; Matsubara, M.; Nishina, S.; Kato, H.; Takaki, A.; Nouso, K.;

Tanaka, T.; Ichimura, K.; Yagi, T.; Yamamoto, K. *Mol. Oncol.* **2013**, *7*, 840−849.
(28) Pratt, S.; Shepard, R. L.; Kandasamy, R. A.; Johnston, P. A.; Perry, W., III; Dantzig, A. H. *Mol. Cancer Ther.* **2005**, *4*, 855−863.